Soluble Conjugated Polymers without Side Chains: Macrocycles as Comonomers

Martina Rimmele,[‡a] Stefania Moro,[‡b] Troy L. R. Bennett,[a] James M. Turner,[c] Filip Aniés,[d] Qiao He,[a] Andrew J. P. White,[a] Simon E. F. Spencer,[e] Martin Heeney,[a,d] Felix Plasser,[c] Giovanni Costantini,[b] Florian Glöcklhofer[*a,f]

[a] Department of Chemistry & Centre for Processable Electronics, Molecular Sciences Research Hub, Imperial College London, London W12 0BZ, United Kingdom

[b] School of Chemistry, University of Birmingham, Birmingham, B15 2TT, United Kingdom

[c] Department of Chemistry, Loughborough University, Loughborough LE11 3TU, United Kingdom

[d] Physical Sciences and Engineering Division, King Abdullah University of Science and Technology, Thuwal 23955-6900, Saudi Arabia

[e] Department of Statistics, University of Warwick, Coventry CV4 7AL, United Kingdom

[f] Institute of Applied Synthetic Chemistry, TU Wien, Getreidemarkt 9/163, 1060 Vienna, Austria

* florian.gloecklhofer@tuwien.ac.at, f.glocklhofer@imperial.ac.uk; ‡ These authors contributed equally.

Keywords: *conjugated polymers, conjugated macrocycles, solubility, side chains, aromaticity, concealed antiaromaticity, cyclic voltammetry, scanning tunneling microscopy, electrospray deposition, sequencing, visualization of chemical shielding tensors*

Abstract

Solubility and processability play critical roles in the practical application of conjugated polymers, in addition to their optoelectronic properties. Enhancing these features is normally accomplished by attaching aliphatic side chains to the polymer backbone, which, however, can come at the expense of other desirable properties, such as charge carrier mobility and crystallinity. Here, we present a promising alternative approach: incorporating conjugated macrocycles into the conjugated polymer backbone. To demonstrate this approach, we synthesized two novel macrocycle-containing polymers, poly(PCT-T) and poly(PCT-2T), which we found to be soluble in chloroform despite not featuring any aliphatic side chains. The polymers displayed minimal structural defects as well as high conformational flexibility and a tendency towards linearity, as confirmed by electrospray deposition scanning tunneling microscopy, and promising photophysical and electrochemical properties, with computational modeling confirming retained macrocycle functionality. The presented approach unlocks a new avenue for the design of solution-processable conjugated polymers with enhanced performance in organic battery electrodes and (opto)electronic devices.

Introduction

Solubility plays a crucial role in the synthesis and application of conjugated polymers. It allows for processing of the polymers and fabrication of thin films, coatings, and electronic devices using solution-based techniques, such as spin coating or printing.[1,2] For conjugated polymers, processability is normally achieved by attaching aliphatic side chains to the conjugated backbone that promote solubility in organic solvents.[3-5] However, this approach is not without drawbacks. The introduction of aliphatic side chains can decrease the charge carrier mobility, reduce crystallinity, and alter the optical and electronic properties of the polymers, often necessitating tedious optimization of the side chain types and positions to balance solubility and desired performance characteristics.[6-9] This can be rationalized by the fundamental role that side chains play in determining the polymer microstructure, with even minor structural or chemical changes having been shown to dramatically affect the assembly, ordering, and crystallinity of conjugated polymer thin films.[6,10-12] Moreover, when conjugated polymers are used as organic battery electrode materials, the attachment of aliphatic side chains has a detrimental effect on the specific capacity, as the side chains increase the molecular weight without contributing to the capacity.

As a potential alternative to the attachment of side chains, there are reports indicating that macrocyclization can increase the solubility of conjugated molecules.[13-17] For molecules with alternating *p*-phenylene and vinylene units, as known from the iconic class of conjugated polymers poly(*p*-phenylene vinylene)s (PPVs),[18-20] this solubilizing effect appears to be particularly strong: PPVs without side chains cannot be dissolved and processed from solution.[18] Even for oligomers with only four phenylene units (Scheme 1, top left), extremely low solubility has been observed, with the solubility of the reported *E*-isomer found to be insufficient for ^{1}H NMR measurements.[21] In contrast, the corresponding macrocycle, paracyclophanetetraene (PCT; Scheme 1, top center), dissolves well in various organic solvents and the compound can be easily processed from solution.[17,22,23]

Furthermore, conjugated macrocycles can also act as redox-active units,[17,24-29] meaning that, unlike the attachment of aliphatic side chains, macrocyclization may even increase the specific capacity for use as a battery electrode material. In the case of PCT and its derivatives, the macrocyclic structure enables switching between a stable, locally aromatic neutral state (with concealed antiaromaticity) and a stable, globally aromatic doubly charged state (Scheme 1, top right), providing these macrocycles with excellent redox properties.[17,22,23,30-33] The macrocyclic

geometry has also been shown to result in a high degree of porosity of the single crystals of these molecules,[17,32] another valuable feature for battery electrodes and other applications.[34-38]

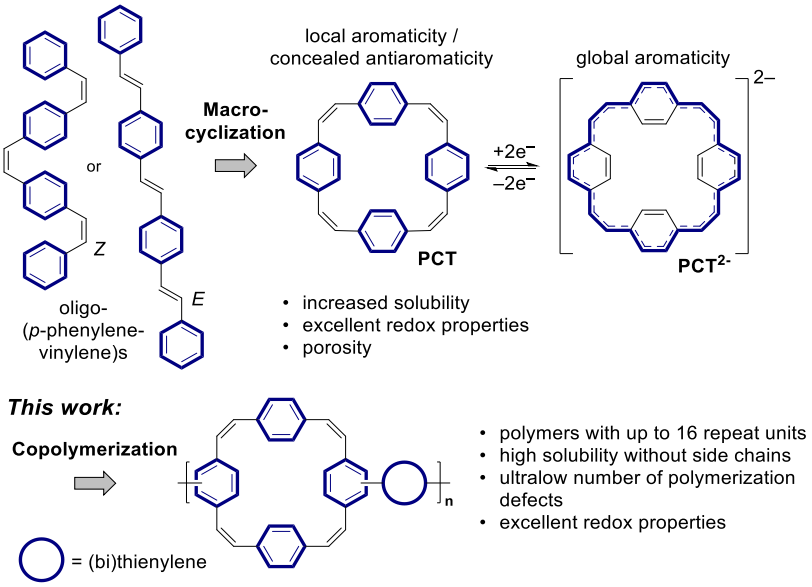

Scheme 1. Top: Molecular design of paracyclophanetetraene (PCT) by macrocyclization of oligo(*p*-phenylenevinylene)s. **Bottom:** Integration of PCT into conjugated polymers by copolymerization with (bi)thiophene derivatives, as reported in this work.

Hence, aiming to achieve solubility and processability of conjugated polymers without the attachment of aliphatic side chains (while also retaining or improving the redox properties), we decided to integrate macrocycles into conjugated polymer backbones. Due to the high solubility and intriguing material properties of PCT and its derivatives, PCT units were chosen as the macrocyclic units and integrated into conjugated polymers by copolymerization with (bi)thiophene derivatives (Scheme 1, bottom).

Results and discussion

Synthesis

For the synthesis of our two target polymers, poly(PCT-T) and poly(PCT-2T) (Figure 1a), we opted for a Stille coupling polymerization reaction, requiring (di)halogenated and (di)stannylated monomers. While the distannylated thiophene and bithiophene comonomers could be sourced from commercial suppliers, dihalogenated PCT was synthesized following our recently reported protocol,[22] which gives dibrominated PCT (diBr-PCT) as a mixture of two regioisomers, namely *trans*-diBr-PCT and *cis*-diBr-PCT (Figure 1a, left). As previous attempts to separate the two regioisomers were unsuccessful, diBr-PCT was deployed as an

isomeric mixture in our polymerization reactions. The ratio of the two regioisomers was estimated to be 1:1.06 from the ^{1}H NMR integrals of the peaks assigned to the phenylene-Hs next to the bromine atom as well as the peaks assigned to the phenylene-Hs of the unsubstituted phenylene units (Figure S2). Both types of phenylene-Hs gave the same ratio.

Interestingly, although previous attempts to separate the two isomers were unsuccessful, slow evaporation of a diBr-PCT solution in a mixture of *n*-hexane and dichloromethane gave a single crystal composed of regiopure *trans*-diBr-PCT, as shown by X-ray diffraction analysis (Figure 1b, CCDC 2335902).

The Stille polymerization reactions were carried out in chlorobenzene using $Pd_2(dba)_3$ and P(*o*-tol)$_3$ for catalysis. For the work-up, the reaction mixtures were precipitated in methanol and purified by Soxhlet extraction with methanol, acetone, hexane, and – for dissolving the polymers – chloroform. The polymers were then reprecipitated in methanol, giving poly(PCT-T) and poly(PCT-2T) as yellow solids in yields of 61% and 94%, respectively. The excellent solubility observed when dissolving the polymers in $CDCl_3$ for ^{1}H NMR measurements (Figures S4 and S6) provided a first indication that the strategy of integrating macrocycles into the backbone of conjugated polymers to achieve solubility was successful.

The molecular weight of the polymers was analyzed by gel permeation chromatography (GPC) in chloroform as well as by matrix-assisted laser desorption ionization mass spectrometry (MALDI-MS) (Table 1). For poly(PCT-T), GPC indicated a number-average molecular weight (M_n) of 1.4 kDa and a weight-average molecular weight (M_w) of 2.0 kDa relative to polystyrene standards. For poly(PCT-2T), a slightly lower M_n of 1.2 kDa but a higher M_w of 2.6 kDa was found. The MALDI-MS measurements (Figure 1c) were in good agreement with these results, with peaks observed at *m/z* values corresponding to up to eight repeat units for poly(PCT-T) and up to six repeat units for poly(PCT-2T). Interestingly, the main peaks observed in the MALDI-MS spectra correspond to multiples of the mass of the repeat unit, without any additional end groups present (Table S2). When analyzing the much smaller side peaks (Table S3), the difference in *m/z* to the main peaks corresponds to additional thiophene/bithiophene or PCT units, with only very weak peaks indicating some presence of bromo or stannyl groups. The fact that residual bromo groups are largely absent in the polymers may explain why no higher molecular weight polymers were obtained. Stille coupling reactions of halogenated phenyl units are known to suffer from reduced reactivity compared to more electron-deficient units,[40] increasing the probability of dehalogenation reactions. The polymers did not precipitate

during the polymerization reaction, indicating that precipitation is not the limiting factor for the molecular weight in this reaction. When testing other Stille polymerization conditions for the synthesis of poly(PCT-T), similar molecular weights were obtained (see Supporting Information section 2.4).[41] However, both poly(PCT-T) and poly(PCT-2T) clearly showed the macroscopic behavior expected for conjugated polymers, including when spin coating and precipitating the polymers. Both polymers were found to be amorphous in powder X-ray diffraction (PXRD) measurements as well as in grazing-incidence wide-angle X-ray scattering (GIWAXS) measurements of spin-coated polymer thin films (see Supporting Information section 6). The thermal properties of the polymers were studied by TGA and DSC, and both polymers showed featureless DSC thermograms, which is indicative of amorphous conjugated polymers (see Figure S12).

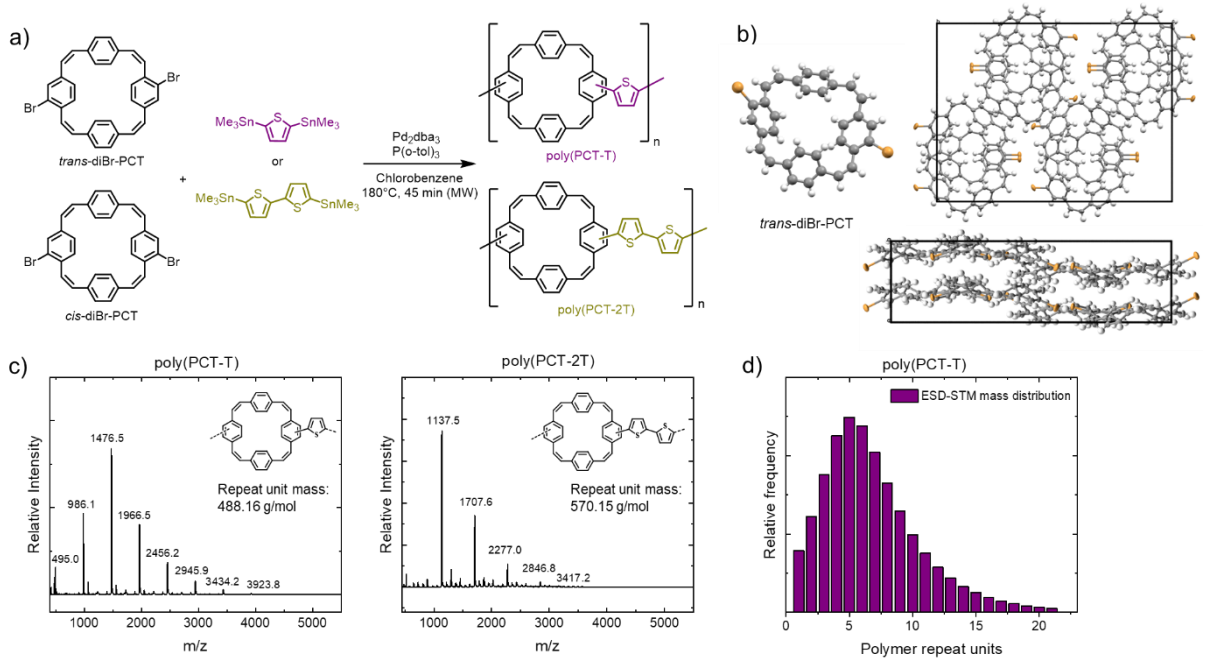

Figure 1. (a) Synthesis of poly(PCT-T) and poly(PCT-2T) by Stille polymerization reactions of an isomeric mixture of *cis*- and *trans*-diBr-PCT and distannylated thiophene and bithiophene derivatives, respectively. (b) Single crystal structure and packing of *trans*-diBr-PCT. (c) Mass spectra of poly(PCT-T) and poly(PCT-2T) obtained from MALDI-MS measurements. (d) ESD-STM-derived mass distribution of poly(PCT-T).

Table 1. Results of molecular weight analyses of poly(PCT-T) and poly(PCT-2T) by GPC, MALDI-MS and ESD-STM, including the number-average (M_n) and weight-average (M_w)

molecular weight as well as the number-average (X_n) and weight-average (X_w) degree of polymerization.

	GPC		MALDI-MS		ESD-STM			
	M_n (kDa)	M_w (kDa)	M_n (kDa)	M_w (kDa)	M_n (kDa)	M_w (kDa)	X_n	X_w
poly(PCT-T)	1.4	2.0	1.8	2.0	3.3	4.5	6.8	9.2
poly(PCT-2T)	1.2	2.6	1.7	1.9	n/a	n/a	n/a	n/a

For poly(PCT-T), an in-depth analysis by electrospray deposition scanning tunnelling microscopy (ESD-STM, see below) offered additional insight into the molecular weight distribution (see also Supporting Information section 9.3). ESD-STM has recently emerged as a methodology for precise mass distribution determination in conjugated polymers, not being affected by aggregation issues and not limited to low-mass samples, unlike GPC or MALDI-MS.[42,43] With an M_n of 3.3 kDa and an M_w of 4.5 kDa (Table 1 right, corresponding to a polydispersity index of 1.36), the actual molecular weight was found to be considerably higher than that indicated by both GPC and MALDI-MS. The difference likely relates to more difficult ionization and desorption of higher molecular weight polymers in the MALDI-MS measurement, and to differences in hydrodynamic volume for poly(PCT-T) versus the polystyrene standard for GPC. Furthermore, while the number- (X_n) and weight-average (X_w) degree of polymerization of the 331 polymer chains analyzed by ESD-STM was 6.8 and 9.2, respectively, polymer chains with up to 16 repeat units were observed in STM images. The STM-derived mass distribution is shown in Figure 1d.

While the degree of polymerization of 6.8 (X_n) and 9.2 (X_w) may be considered low for a polymer, we would like to emphasize that the macrocyclic monomer itself is already an oligomer. Furthermore, for some applications, in particular as redox-active material in battery electrodes, high molecular weights are not crucial for excellent performance.

Solubility

To quantify the solubility in chloroform, a solvent often used for device fabrication, we initially used a stepwise solvent addition approach (see Supporting Information section 8.1). Using this approach, the solubility limit was determined to be approx. 143 mg/mL for poly(PCT-T) and 67 mg/mL for poly(PCT-2T), significantly higher than the polymer concentrations of around

20 mg/mL that are commonly used for optoelectronic device fabrication. As expected, the solubility limit was found to be lower for poly(PCT-2T), as the copolymerization with bithiophene instead of thiophene derivatives results in a lower number of solubilizing units per molecular weight. Similar effects have been observed for polymers incorporating aliphatic side chains.[44]

As an alternative independent evaluation of the polymer solubility, we also employed a previously reported method based on UV/vis absorbance values (see Supporting Information section 8.2),[45] obtaining a solubility limit of 176 mg/mL for poly(PCT-T), in good agreement with the results of the stepwise solvent addition approach.

Polymer sequence and conformation

To investigate the polymer sequence and conformations at the single-molecule level, we employed ESD-STM. This advanced methodology, developed in recent years, enables the imaging of polymeric assemblies with sub-molecular resolution while avoiding issues related to aggregation and high-mass limitations.[12,42,43,46,47] Poly(PCT-T) was vacuum deposited by ESD on a Au(111) surface at sub-monolayer coverages and analyzed in ultrahigh vacuum by STM.

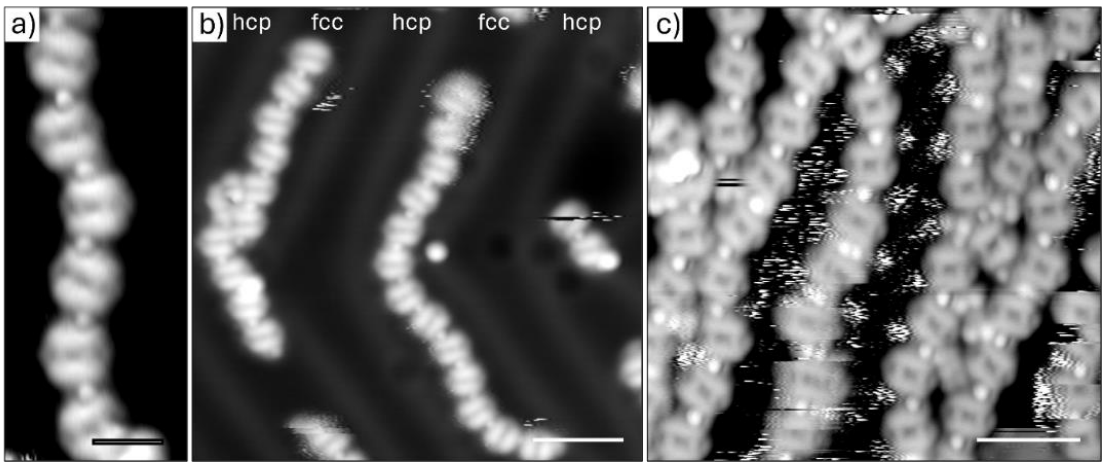

Figure 2. (a) In the STM images, poly(PCT-T) appears as an alternation of small round beads (thiophene units) and larger rectangular shapes (PCT units). (b) At low surface density, the polymers adsorb on the fcc areas of the substrate and are elongated, following the template of the herringbone reconstruction of Au(111), without significant interaction with other polymers. (c) At higher densities, poly(PCT-T) creates more compact islands, with polymers laterally interacting with one another. The scale bars represent: (a) 2 nm; (b) 4 nm; (c) 3 nm.

The polymers are oriented face-on with respect to the substrate and appear as linear chains of alternating smaller, circular, and larger, rectangular features that are identified as thiophene and PCT units, respectively (Figure 2a). In low molecular density areas of the sample, the polymers adsorb preferentially in the face-centered cubic (fcc) regions of the Au(111) herringbone reconstruction (Figure S16),[48-50] and follow its templating pattern, avoiding interacting with one another (Figure 2b and, for a larger scale, Figure S17). The potential energy barriers between different areas of the herringbone reconstruction act as an adsorption well to confine the polymers, that would otherwise be quite mobile under the STM tip (see for example Figure S18 for a comparison of more/less constrained polymers). The polymers have the conformational flexibility to form bends to accommodate for the templating effect of the substrate but remain generally elongated.

In higher molecular density regions, while the surface confinement to fcc areas is still observed, the polymers adsorb also in the hexagonal close packed (hcp) areas of the substrate and/or cross the dislocation lines of the herringbone reconstruction. At these higher concentrations, the polymers can laterally interact, forming local closed-packed arrangements (Figure 2c).

Geometry-optimized molecular models of the monomers were created by using the MMFF94s force field in Avogadro[51] and used to represent the polymer structures in the STM images. While the details of the fitting of the STM images are discussed in the Supporting Information section 9.1, this procedure allowed us to directly sequence the polymer backbones, as shown in Figure 3. In particular, we measured the frequencies of *cis*- and *trans*-PCT isomers within the polymers, obtaining a 1:1.26 ratio over a total of 822 isomers. This is statistically significantly different from the 1:1.06 ratio measured by NMR for the isolated dibrominated monomers, indicating that the *trans* monomers are incorporated in the polymer sequences with higher probability. The two regioisomers are, however, distributed independently along the backbone, as demonstrated by a statistical test of significance (see Supporting Information section 9.2 for a detailed discussion).

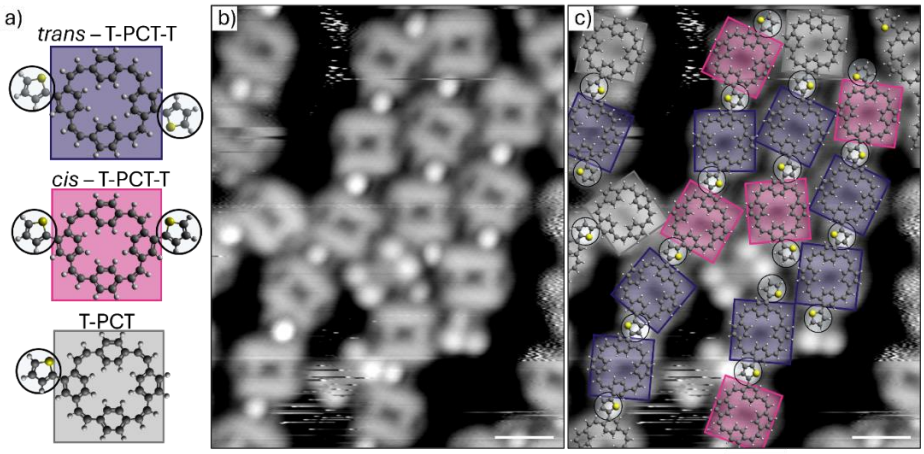

Figure 3. (a) Models of T-PCT-T in *trans* (macrocycle in blue) and *cis* conformation (macrocycle in pink). Thiophene units are marked with black circles. Macrocycles for which one of the two flanking thiophenes is not visible are shown in gray (T-PCT). (b) High-resolution STM image of poly(PCT-T). (c) Geometry-optimized molecular models of the repeat units overlayed to the STM image in (b). Squares and circles follow the legend in (a). For *trans* isomers, the two flanking thiophenes are located across the diagonal of the square, while for *cis* isomers they are located on the same side of the backbone axis. The scale bars represent 1 nm.

The absence of any regioisomer segregation and the high conformational flexibility imparted to poly(PCT-T) by the single C-C bonds between the thiophene and the PCT units (Figure S20) explain why these molecules can adopt an overall straight geometry, as observed in the STM images. Even though the specific arrangement of the polymer in 3D may vary from what is observed for its adsorption on Au(111), our 2D results still demonstrate a tendency towards linearity of poly(PCT-T). This suggests that its high solubility is not due to a highly kinked polymer structure that would impede intermolecular packing and aggregation.

The sequencing of a large set of polymers also allowed us to analyze the polymer ends, showing that in 84% of cases the polymers are terminated by a thiophene unit, and only in 16% by a PCT comonomer. Moreover, a similar statistical analysis of the polymer sequences demonstrated that, at variance with other cases of cross-coupling polymerizations,[43,52,53] the synthetic approach used here for making poly(PCT-T) is highly defect-free, as only extremely rare examples of homocoupling defects were observed. Thiophene homocouplings (Figure 4a and 4b) accounted for 0.2% of all measured bonds (over a total of 2585), while only a single case of PCT-PCT coupling was observed overall, corresponding to a relative frequency $< 0.05\%$ (Figure 4c and 4d). In this latter case, the two PCT macrocycles forming the defect

appear distorted in the STM images, which is possibly a sign of a spatial deformation due to steric hindrance upon adsorption.

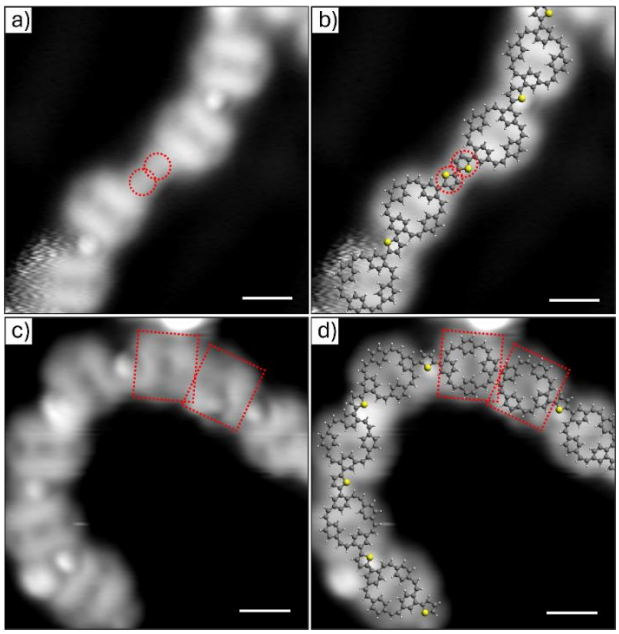

Figure 4. (a) Polymer presenting a thiophene-thiophene homocoupling defect (red dotted circles). The corresponding fit is shown in (b). (c) Polymer presenting a PCT-PCT homocoupling (red dotted rectangles) and corresponding molecular fit in (d). The scale bars represent 1 nm.

Interestingly, a small percentage of polymer chains were seen to close over themselves (Figure S19). While STM cannot directly prove the cyclization, the fact that these cycles are adsorbed across the herringbone reconstruction and are not seen to move under the STM probe during scanning suggests the presence of a strong intramolecular bond. These polymers or cycles are composed of 7 to 15 repeat units, displaying a whole distribution of values.

Photophysical and electrochemical properties

The photophysical and electrochemical properties of poly(PCT-T) and poly(PCT-2T) were investigated by UV/vis absorption and photoluminescence (PL) spectroscopy as well as cyclic voltammetry (CV) (Figure 5) and compared to the properties of PCT. The key characteristics obtained from these measurements are summarized in Tables 2 and 3. Solution UV/vis absorption measurements were performed in $CHCl_3$ (solid lines in Figure 5a), showing one absorption band with a maximum at 305 nm for poly(PCT-T) and two absorption bands with maxima at 308 nm and 374 nm for poly(PCT-2T), with the (first) absorption maximum being

almost identical to the absorption maximum of PCT at 306 nm. Similar observations were made in the thin film measurements (Figure 5b), with absorption maxima at 318 nm for PCT, 330 nm for poly(PCT-T), and 314 nm and 379 nm for poly(PCT-2T). However, significant peak broadening and a drastic redshift of the absorption onset was observed in the thin films. The rather large optical gaps ($E_{g,opt}$) in solution of 3.2 eV for poly(PCT-T) and 2.7 eV for poly(PCT-2T), determined from the absorption onsets, are drastically reduced in the solid state, with an absorption tail to approximately 700 nm (corresponding to 1.8 eV) found for poly(PCT-2T). This substantial redshift can serve as evidence for significant intermolecular interactions of the polymer chains in the solid state.

The PL spectra of the polymers in $CHCl_3$ (dashed lines in Figure 5a) were recorded upon excitation at the absorption maximum wavelengths of 305 and 308 nm, respectively. Poly(PCT-T) exhibited a PL maximum at 486 nm and poly(PCT-2T) at 512 nm, both redshifted compared to the PL maximum of PCT at 472 nm. As PCT, both polymers showed substantial Stokes shifts, leading to almost no overlap between absorption and PL bands.

The electrochemical properties of poly(PCT-T), poly(PCT-2T) and PCT were also analyzed in both solution and film, using the ferrocene/ferrocenium (Fc/Fc^+) redox couple as an internal reference. Solution voltammograms were recorded in a DMF-[*n*-Bu_4N]PF_6 electrolyte (0.1 M), showing reversible reduction processes for both polymers at redox potentials of –2.13 and –2.10 V *vs.* Fc/Fc^+, respectively (Figure 5c). These values are very similar to the redox potential of –2.09 V found for the reversible two-electron reduction of bare PCT to the globally aromatic dianion in the same electrolyte, as well as to the redox potentials for the corresponding reduction of thiophene-substituted PCT derivatives.[22] For the film measurements (Figure 5d), the polymers and PCT were deposited directly onto a glassy carbon electrode and measured in an acetonitrile-[*n*-Bu_4N]PF_6 electrolyte (0.1 M). As in solution, both polymers exhibited reversible reduction processes, albeit with a slightly larger difference in redox potentials. This is in sharp contrast to the film measurement of PCT, where the reduced PCT dianion dissolved in the electrolyte, preventing back oxidation to the neutral state. The film measurements revealed a redox potential of –2.26 V for poly(PCT-2T) and –2.08 V for poly(PCT-T), similar to the redox potential of –2.19 V found for PCT. In contrast to the reduction, the oxidation of the polymers at approx. 0.7 V was found to be irreversible in both cases.

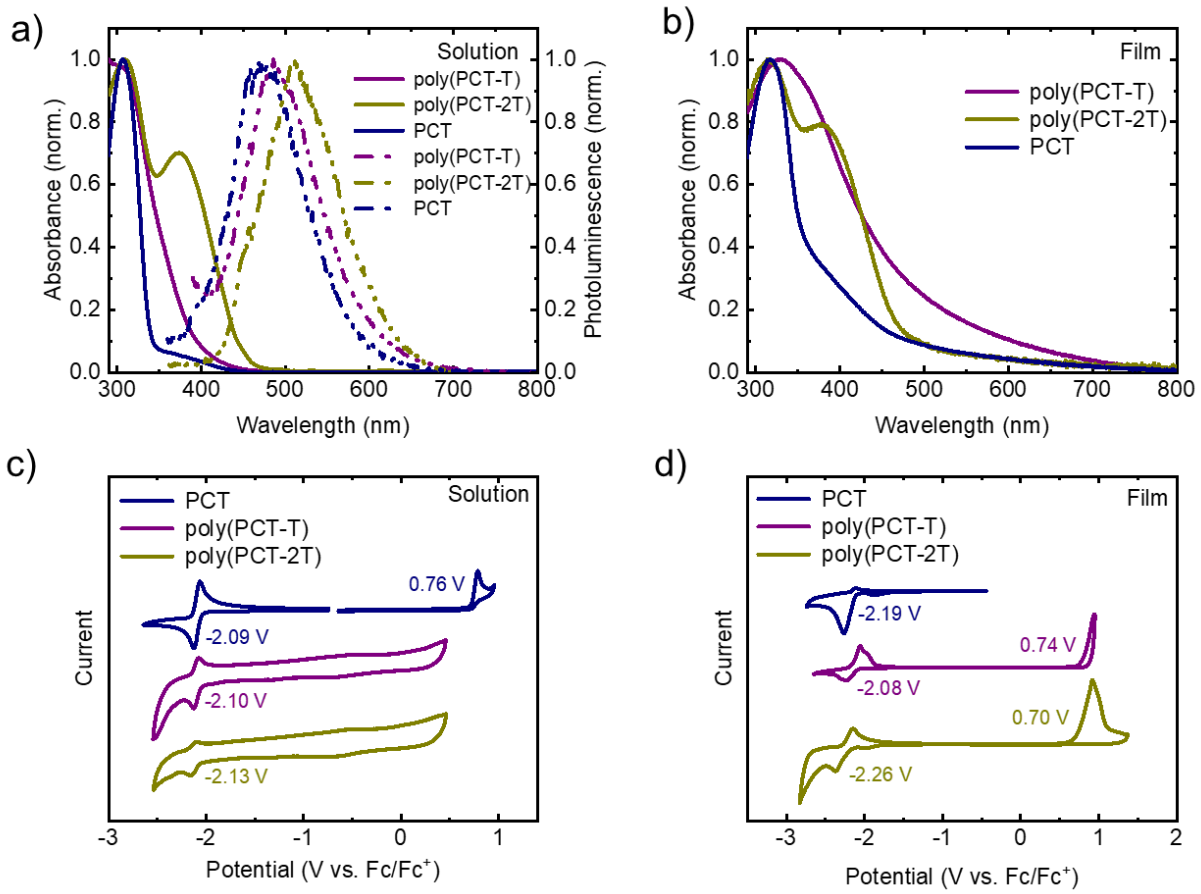

Figure 5. Photophysical and electrochemical characterization of PCT, poly(PCT-T) and poly(PCT-2T) in solution and film. (a) UV/vis absorption (solid line) and PL (dashed line) spectra in $CHCl_3$ solutions. (b) UV/vis absorption of thin films spin-cast from $CHCl_3$ solutions. Cyclic voltammograms of PCT and the polymers in (c) DMF solutions and (d) films dropcast onto a glassy carbon electrode. 0.1 M [*n*-Bu_4N]PF_6 solutions in either DMF (solution) or acetonitrile (thin film) were used as the supporting electrolyte.

Table 2. Key photophysical characteristics of the polymers in $CHCl_3$ solution and thin films obtained from UV/vis and PL measurements.

	$\lambda_{max,abs}$ (solution) (nm)	$\lambda_{max,abs}$ (film) (nm)	$\lambda_{max,PL}$ (solution) (nm)	Stokes shift (eV)
poly(PCT-T)	305	330	486	1.51
poly(PCT-2T)	308	314	512	1.60
PCT	306	318	472	1.42

Table 3. Key electrochemical characteristics of the polymers in DMF solution and thin films, obtained from CV measurements.

		Reduction potential (V *vs.* Fc/Fc^+)	Oxidation potential (V *vs.* Fc/Fc^+)	Estimated LUMO (eV)	Estimated HOMO (eV)	E_g (eV)
poly(PCT-T)	solution	–2.13		–2.67		
	film	–2.08	0.74	–2.72	–5.54	2.82
poly(PCT-2T)	solution	–2.10		–2.70		
	film	–2.26	0.70	–2.54	–5.50	2.96
PCT	solution	–2.09	0.76	–2.71	–5.56	2.85
	film	–2.19		–2.61		

Computational analysis

The similarity in redox behavior between the polymers and bare PCT as well as thiophene-substituted PCT derivatives provided some indication that the ability of the PCT units to become globally aromatic (cf. Scheme 1, top right) is not affected by the integration into the conjugated polymer backbone. To study the effect of neighboring PCT units on the redox behavior and on the local and global aromaticity in different charge and spin states in more detail, we computed the redox potentials and carried out nucleus-independent chemical shift (NICS)[54] calculations for polymer fragments composed of two PCT units linked by either a thiophene (PCT-T-PCT, Figure 6) or bithiophene unit (PCT-2T-PCT, Supporting Information section 10.3.2). The NICS tensors were then represented graphically using the visualization of chemical shielding tensors (VIST) method.[55] The results of these computations on PCT-T-PCT, which consider the neutral ground state, the doublet monoanion, the singlet and triplet of the dianion, the doublet trianion as well as the singlet and triplet of the tetraanion, are presented and discussed here.

The first remarkable observation is the similarity of all the redox potentials. Except for the reduction to the triplet tetraanion, all redox potentials lie within –1.9 and –2.3 V *vs.* Fc/Fc^+, meaning that all reduction steps from the neutral molecule to the tetraanion may occur in a single reduction wave in CV experiments, and the obtained range matches well with the

experimental value of –2.1 V. In other words, one would expect a concerted four-electron reduction for the dimer and a concerted two-electron reduction of all PCT units for the polymer.

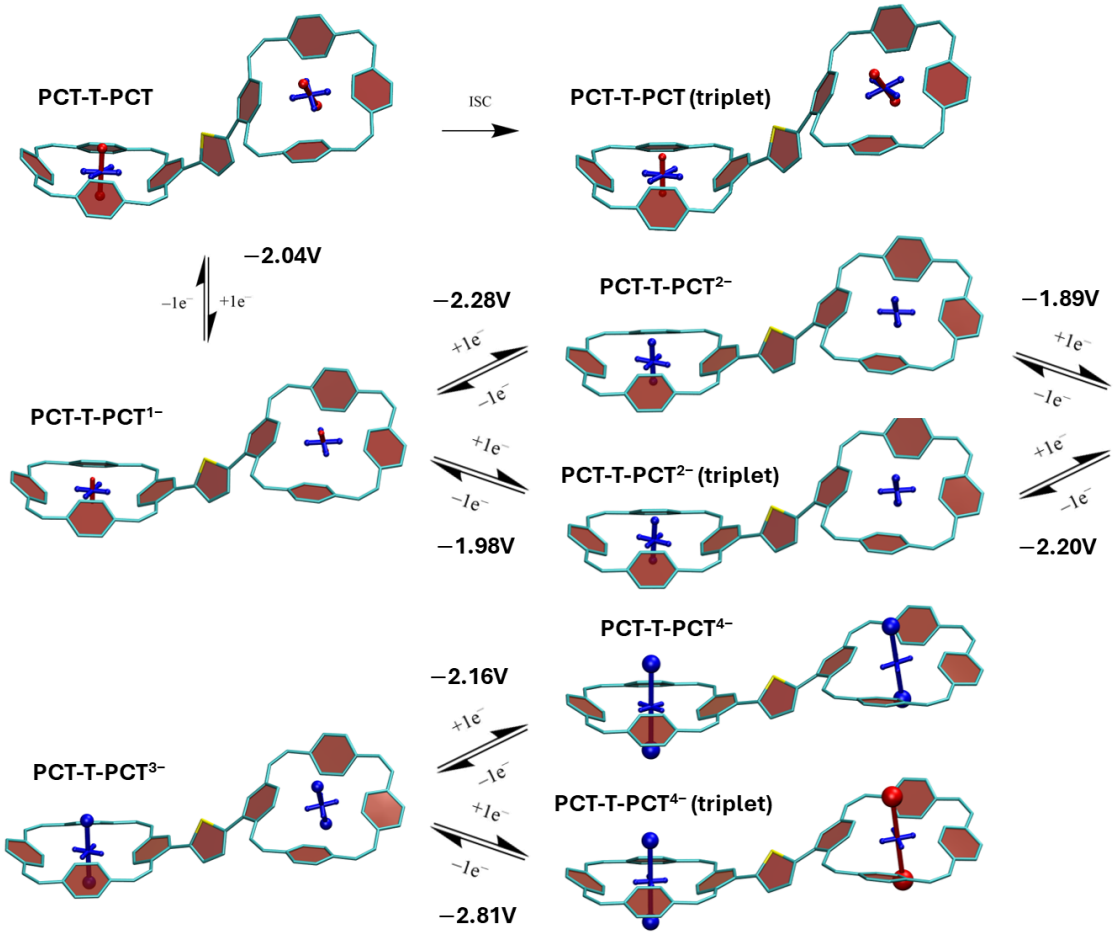

Figure 6. Analysis of various electronic states of PCT-T-PCT going from the neutral state to the triplet excited state (top) then to the monoanion and dianion (middle) to trianion and tetraanion (bottom). Computed redox potentials are presented along with the individual redox steps. Magnetic properties are represented via VIST plots with shielded (aromatic) components shown in blue and deshielded (antiaromatic) components shown in red.

Moving on to the VIST plots, we first note the small deshielded (red) tensor components (+9.3 and +10.2 ppm) in the case of the neutral dimer. In line with previous discussions,[55] we assign the deshielding as deriving from the diatropic currents in the phenylene units rather than indicating global antiaromaticity. As mentioned in the introduction, neutral PCT can be seen as a molecule with concealed antiaromaticity, considering that it possesses $4n$ π-electrons along its perimeter but that it relaxes into a geometry where the macrocyclic conjugation is weakened. Viewing the subsequent reduced states, we find (with the exception of the triplet tetraanion) enhanced (global) aromaticity in the PCT units with increasing number of electrons. The

monoanion becomes more planar than the neutral molecule, a trend that is continued through the reduced states, while also becoming less deshielded as the electron is added. The singlet and triplet dianions exhibit comparatively small shielding (between –6.5 and –8.8 ppm), indicating only minor generation of aromaticity noting that the charge is distributed over both rings. To explain this behavior, it is worth noting that the triplet dianion can be seen as being formed from two independent PCT rings that are both doublet monoanions exhibiting slight global aromaticity. In contrast, the singlet dianion is more closely related to the combination of a dianion PCT with a neutral PCT, and its slightly higher energy can be related to the repulsion of the two electrons within the LUMO of one PCT unit. More pronounced shielding components are seen for the trianion (–16.9 / –21.7 ppm) and singlet tetraanion (–34.1 / –36.4 ppm). The latter values closely resemble the shielding of –38.7 ppm observed for the dianion of isolated PCT, highlighting the minimal influence of the thiophene and second PCT on the electronic structure. Within Figure 6, it is the triplet tetraanion that clearly sticks out. This state is formed as a combination of a singlet and a triplet dianion, where the former is Hückel aromatic and the latter is Baird antiaromatic. Consequently, the triplet tetraanion possesses one strongly aromatic and one strongly antiaromatic ring. The antiaromaticity is also reflected by its more unfavorable redox potential of –2.81 V. Analogous results on PCT-2T-PCT are presented in the Supporting Information section 10. These results are very similar to those obtained for PCT-T-PCT, highlighting the minimal influence of the second thiophene unit.

Similar to our recent investigation of thiophene-substituted PCT derivatives,[22] we also analyzed the electronic structure in detail by computing the natural difference orbitals (NDOs)[56] between the neutral S0 state and the reduced (1−, 2−, 3−, 4−) and excited triplet states (T1). The NDOs can show whether the charge or the excitation is delocalized over the entire molecule, predominantly delocalized over one PCT unit, or localized on a certain part of the molecule. These NDOs are shown in the Supporting Information section 10.4. For the most part, all relevant NDOs have a very similar appearance featuring even delocalization within the PCT units, with 12 nodal planes counted along the perimeter of the PCT units. Crucially, the HOMO and LUMO of the PCT units both possess 12 nodal planes, meaning that they are quasi-degenerate within a simple rotor model, and this fact underscores the formal antiaromaticity of the neutral system and aromaticity of the dianion (see also Ref. 57). Slightly different NDO shapes are obtained for the neutral triplets, which are more localized, as observed previously for related molecules.[31] More strongly divergent NDO shapes are observed for the triplet tetraanions, in line with their altered VIST plots.

Finally, we were interested in studying the effect of the thiophene units in mediating electronic coupling and, thus, delocalization between the PCT units. For this purpose, we computed hole and electron transfer integrals between the PCT units considering PCT-PCT, PCT-T-PCT and PCT-2T-PCT and doing computations on one C_2-symmetric conformer for each (see Table S7). The hole/electron transfer integrals for PCT-PCT, with directly linked PCT units, were computed as 4/93 meV, indicating some potential of the LUMO to delocalize across the two molecules but also showing that the two units are already mostly decoupled. Including one or two thiophene spacers to produce PCT-T-PCT and PCT-2T-PCT yielded hole/electron transfer integrals of 34/35 and 29/14 meV, respectively. This highlights that electron transfer integrals are lowered, whereas the hole transfer integrals are slightly going up, possibly due to the electron-rich nature of the thiophene spacer. We should note that the precise value of the transfer integrals is expected to vary with different conformers.

In summary, the computations highlight that the PCT units in the dimer (and, by extension, the polymer) act mostly like isolated PCT units in redox reactions and that they are largely decoupled, once the thiophene spacer units are included.

Conclusions

Our work demonstrates a new strategy for achieving solubility and processability of conjugated polymers by incorporating conjugated macrocycles directly into the polymer backbone, eliminating the need to attach side chains. This approach is exemplified by the synthesis of two novel macrocycle-containing conjugated polymers, poly(PCT-T) and poly(PCT-2T), which were found to be soluble in chloroform despite lacking any side chains. ESD-STM analysis of poly(PCT-T) revealed an ultralow number of structural defects, a high degree of conformational flexibility, and a preference for linear conformations, indicating that the high solubility is not due to a highly kinked or irregular polymer structure that would impede intermolecular packing and aggregation. The STM analysis further indicated a random distribution of *cis*- and *trans*-PCT isomers along the polymer backbone and a preference for the incorporation of *trans*-PCT isomers. Interestingly, a small percentage of polymer chains were observed to close over themselves, suggesting the formation of cycles composed of up to 15 repeat units. Both powders and spin-coated thin films of poly(PCT-T) and poly(PCT-2T) were found to be amorphous in PXRD and GIWAXS measurements. Furthermore, the polymers possess promising photophysical and electrochemical properties, with computational modeling confirming the retention of macrocycle functionality upon integration into the

backbone, where the thiophene spacers serve to further decouple the individual macrocycles. In particular, the macrocycles appear to retain their ability to become globally aromatic upon reduction even when integrated into polymer backbones. However, as a key advantage over PCT, the polymers did not dissolve in the polar, acetonitrile-based electrolyte used for film CV measurements, neither in the neutral nor in the reduced state, enabling reversible redox behavior in solid-state applications. While the relatively low degree of polymerization may play a role in ensuring solubility in less polar solvents (in addition to the solubilizing effect of macrocyclization), this shows that we can access desirable properties of conjugated polymers even without a high degree of polymerization. Hence, we are confident that our findings pave the way for the rational design of novel solution-processable conjugated polymers with superior properties for applications in organic battery electrodes and (opto)electronic devices. As the molecular weight of the polymers was not limited by precipitation during the reaction, we expect that higher molecular-weight polymers can be obtained by developing macrocyclic monomers with higher reactivity in polymerization reactions. Future work will also need to investigate the generality of the approach to soluble conjugated polymers introduced in this work.

Supporting Information

Results and details regarding instrumentation, synthesis, NMR spectroscopy, crystallography, molecular weight determination, morphology analysis, thermal analysis, solubility determination, scanning tunneling microscopy (STM), and computations.

Acknowledgement

This work was supported by the Austrian Science Fund (FWF), under project number J 4463, and the EPSRC, grant EP/V048686/1. M. R. acknowledges support from the EPSRC (EP/R513052/1). J. M. T. acknowledges support by the SusHy CDT (EPSRC grant EP/S023909/1). S. M. and G. C. acknowledge support from a UK – Saudi Challenge Fund grant from the British Council's Going Global Partnerships Programme. AI tools were used to obtain first drafts of the abstract and conclusions section. We would like to thank Alla Dikhtiarenko (Core Labs, King Abdullah University of Science and Technology) for PXRD measurements.

Author contributions

The manuscript was written through contributions of all authors. All authors have given approval to the final version of the manuscript.

References

1. Forrest, S. R., The path to ubiquitous and low-cost organic electronic appliances on plastic, *Nature* **2004**, *428* (6986), 911-918. DOI:10.1038/nature02498
2. Choudhary, K.; Chen, A. X.; Pitch, G. M.; Runser, R.; Urbina, A.; Dunn, T. J.; Kodur, M.; Kleinschmidt, A. T.; Wang, B. G.; Bunch, J. A.; Fenning, D. P.; Ayzner, A. L.; Lipomi, D. J., Comparison of the Mechanical Properties of a Conjugated Polymer Deposited Using Spin Coating, Interfacial Spreading, Solution Shearing, and Spray Coating, *ACS Appl. Mater. Interfaces* **2021**, *13* (43), 51436-51446. DOI:10.1021/acsami.1c13043
3. Guo, X.; Facchetti, A., The journey of conducting polymers from discovery to application, *Nat. Mater.* **2020**, *19* (9), 922-928. DOI:10.1038/s41563-020-0778-5
4. Wang, S.; Shaw, J.; Han, Y.; Fei, Z.; Glöcklhofer, F.; Heeney, M., Multibranched aliphatic side chains for π-conjugated polymers with a high density of 'unshielded' aromatics, *Chem. Commun.* **2020**, *56* (81), 12138-12141. DOI:10.1039/D0CC04967K
5. Elsenbaumer, R. L.; Jen, K. Y.; Oboodi, R., Processible and environmentally stable conducting polymers, *Synth. Met.* **1986**, *15* (2), 169-174. DOI:10.1016/0379-6779(86)90020-2
6. Mei, J.; Bao, Z., Side Chain Engineering in Solution-Processable Conjugated Polymers, *Chem. Mater.* **2014**, *26* (1), 604-615. DOI:10.1021/cm4020805
7. Lei, T.; Wang, J.-Y.; Pei, J., Roles of Flexible Chains in Organic Semiconducting Materials, *Chem. Mater.* **2014**, *26* (1), 594-603. DOI:10.1021/cm4018776
8. Liu, Z.; Zhang, G.; Zhang, D., Modification of Side Chains of Conjugated Molecules and Polymers for Charge Mobility Enhancement and Sensing Functionality, *Acc. Chem. Res.* **2018**, *51* (6), 1422-1432. DOI:10.1021/acs.accounts.8b00069
9. Yang, Y.; Liu, Z.; Zhang, G.; Zhang, X.; Zhang, D., The Effects of Side Chains on the Charge Mobilities and Functionalities of Semiconducting Conjugated Polymers beyond Solubilities, *Adv. Mater.* **2019**, *31* (46), 1903104. DOI:10.1002/adma.201903104
10. Kline, R. J.; DeLongchamp, D. M.; Fischer, D. A.; Lin, E. K.; Richter, L. J.; Chabinyc, M. L.; Toney, M. F.; Heeney, M.; McCulloch, I., Critical Role of Side-Chain Attachment Density on the Order and Device Performance of Polythiophenes, *Macromolecules* **2007**, *40* (22), 7960-7965. DOI:10.1021/ma0709001
11. Hallani, R. K.; Paulsen, B. D.; Petty, A. J., II; Sheelamanthula, R.; Moser, M.; Thorley, K. J.; Sohn, W.; Rashid, R. B.; Savva, A.; Moro, S.; Parker, J. P.; Drury, O.; Alsufyani, M.; Neophytou, M.; Kosco, J.; Inal, S.; Costantini, G.; Rivnay, J.; McCulloch, I., Regiochemistry-Driven Organic

Electrochemical Transistor Performance Enhancement in Ethylene Glycol-Functionalized Polythiophenes, *J. Am. Chem. Soc.* **2021**, *143* (29), 11007-11018. DOI:10.1021/jacs.1c03516

12. Moro, S.; Siemons, N.; Drury, O.; Warr, D. A.; Moriarty, T. A.; Perdigão, L. M. A.; Pearce, D.; Moser, M.; Hallani, R. K.; Parker, J.; McCulloch, I.; Frost, J. M.; Nelson, J.; Costantini, G., The Effect of Glycol Side Chains on the Assembly and Microstructure of Conjugated Polymers, *ACS Nano* **2022**, *16* (12), 21303-21314. DOI:10.1021/acsnano.2c09464
13. Campbell, K.; McDonald, R.; Branda, N. R.; Tykwinski, R. R., Rigid, Cross-Conjugated Macrocycles: A Cyclic Alternative to 4,4‘-Bipyridines in Supramolecular Chemistry, *Org. Lett.* **2001**, *3* (7), 1045-1048. DOI:10.1021/ol0156087
14. Sannicolò, F.; Mussini, P. R.; Benincori, T.; Cirilli, R.; Abbate, S.; Arnaboldi, S.; Casolo, S.; Castiglioni, E.; Longhi, G.; Martinazzo, R.; Panigati, M.; Pappini, M.; Quartapelle Procopio, E.; Rizzo, S., Inherently Chiral Macrocyclic Oligothiophenes: Easily Accessible Electrosensitive Cavities with Outstanding Enantioselection Performances, *Chem. - Eur. J.* **2014**, *20* (47), 15298-15302. DOI:10.1002/chem.201404331
15. Li, P.; Sisto, T. J.; Darzi, E. R.; Jasti, R., The Effects of Cyclic Conjugation and Bending on the Optoelectronic Properties of Paraphenylenes, *Org. Lett.* **2014**, *16* (1), 182-185. DOI:10.1021/ol403168x
16. Kuwabara, T.; Orii, J.; Segawa, Y.; Itami, K., Curved Oligophenylenes as Donors in Shape-Persistent Donor–Acceptor Macrocycles with Solvatofluorochromic Properties, *Angew. Chem., Int. Ed.* **2015**, *54* (33), 9646-9649. DOI:10.1002/anie.201503397
17. Eder, S.; Yoo, D.-J.; Nogala, W.; Pletzer, M.; Santana Bonilla, A.; White, A. J. P.; Jelfs, K. E.; Heeney, M.; Choi, J. W.; Glöcklhofer, F., Switching between Local and Global Aromaticity in a Conjugated Macrocycle for High-Performance Organic Sodium-Ion Battery Anodes, *Angew. Chem., Int. Ed.* **2020**, *59* (31), 12958-12964. DOI:10.1002/anie.202003386
18. Blayney, A. J.; Perepichka, I. F.; Wudl, F.; Perepichka, D. F., Advances and Challenges in the Synthesis of Poly(p-phenylene vinylene)-Based Polymers, *Isr. J. Chem.* **2014**, *54* (5-6), 674-688. DOI:10.1002/ijch.201400067
19. Schönbein, A.-K.; Wagner, M.; Blom, P. W. M.; Michels, J. J., Quantifying the Kinetics of the Gilch Polymerization toward Alkoxy-Substituted Poly(p-phenylene vinylene), *Macromolecules* **2017**, *50* (13), 4952-4961. DOI:10.1021/acs.macromol.7b00697
20. Rimmele, M.; Ableidinger, K.; Marsh, A. V.; Cheetham, N. J.; Taublaender, M. J.; Buchner, A.; Prinz, J.; Fröhlich, J.; Unterlass, M. M.; Heeney, M.; Glöcklhofer, F., Thioalkyl- and sulfone-substituted poly(p-phenylene vinylene)s, *Polym. Chem.* **2019**, *10* (6), 738-750. DOI:10.1039/C8PY01717D
21. Mamada, M.; Nakanotani, H.; Adachi, C., Amplified spontaneous emission from oligo(p-phenylenevinylene) derivatives, *Mater. Adv.* **2021**, *2* (12), 3906-3914. DOI:10.1039/D0MA00756K

22. Bennett, T. L. R.; Marsh, A. V.; Turner, J. M.; Plasser, F.; Heeney, M.; Glöcklhofer, F., Functionalisation of conjugated macrocycles with type I and II concealed antiaromaticity via cross-coupling reactions, *Mol. Syst. Des. Eng.* **2023**, *8* (6), 713-720. DOI:10.1039/D3ME00045A
23. Stawski, W.; Zhu, Y.; Wei, Z.; Petrukhina, M. A.; Anderson, H. L., Crystallographic evidence for global aromaticity in the di-anion and tetra-anion of a cyclophane hydrocarbon, *Chem. Sci.* **2023**, *14* (48), 14109-14114. DOI:10.1039/D3SC04251K
24. Pawlicki, M.; Latos-Grażyński, L., Aromaticity Switching in Porphyrinoids, *Chem. - Asian J.* **2015**, *10* (7), 1438-1451. DOI:10.1002/asia.201500170
25. Kayahara, E.; Kouyama, T.; Kato, T.; Yamago, S., Synthesis and Characterization of [n]CPP (n = 5, 6, 8, 10, and 12) Radical Cation and Dications: Size-Dependent Absorption, Spin, and Charge Delocalization, *J. Am. Chem. Soc.* **2016**, *138* (1), 338-344. DOI:10.1021/jacs.5b10855
26. Zhou, Z.; Wei, Z.; Schaub, T. A.; Jasti, R.; Petrukhina, M. A., Structural deformation and host–guest properties of doubly-reduced cycloparaphenylenes, [n]CPPs2− (n = 6, 8, 10, and 12), *Chem. Sci.* **2020**, *11* (35), 9395-9401. DOI:10.1039/D0SC03072D
27. Varni, A. J.; Kawakami, M.; Tristram-Nagle, S. A.; Yaron, D.; Kowalewski, T.; Noonan, K. J. T., Design, synthesis, and properties of a six-membered oligofuran macrocycle, *Org. Chem. Front.* **2021**, *8* (8), 1775-1782. DOI:10.1039/D1QO00084E
28. Ambhore, M. D.; Panchal, S. P.; Mondal, A.; Konar, S.; Anand, V. G., Reversible redox switching between local and global aromaticity for core-modified expanded carbaisophlorinoids, *Org. Biomol. Chem.* **2022**, *20* (14), 2818-2821. DOI:10.1039/D1OB02230J
29. Rahav, Y.; Rajagopal, S. K.; Dishi, O.; Bogoslavsky, B.; Gidron, O., Alternating behavior in furan-acetylene macrocycles reveals the size-dependency of Hückel's rule in neutral molecules, *Communications Chemistry* **2023**, *6* (1), 100. DOI:10.1038/s42004-023-00902-9
30. Rimmele, M.; Nogala, W.; Seif-Eddine, M.; Roessler, M. M.; Heeney, M.; Plasser, F.; Glöcklhofer, F., Functional group introduction and aromatic unit variation in a set of π-conjugated macrocycles: revealing the central role of local and global aromaticity, *Org. Chem. Front.* **2021**, *8* (17), 4730-4745. DOI:10.1039/D1QO00901J
31. Pletzer, M.; Plasser, F.; Rimmele, M.; Heeney, M.; Glöcklhofer, F., [2.2.2.2]Paracyclophanetetraenes (PCTs): cyclic structural analogues of poly(p-phenylene vinylene)s (PPVs) [version 2; peer review: 2 approved], *Open Res. Europe* **2022**, *1*, 111. DOI:10.12688/openreseurope.13723.2
32. Eder, S.; Ding, B.; Thornton, D. B.; Sammut, D.; White, A. J. P.; Plasser, F.; Stephens, I. E. L.; Heeney, M.; Mezzavilla, S.; Glöcklhofer, F., Squarephaneic Tetraanhydride: A Conjugated Square-Shaped Cyclophane for the Synthesis of Porous Organic Materials, *Angew. Chem., Int. Ed.* **2022**, *61* (48), e202212623. DOI:10.1002/anie.202212623

33. Ding, B.; Bhosale, M.; Bennett, Troy L. R.; Heeney, M.; Plasser, F.; Esser, B.; Glöcklhofer, F., Reducing undesired solubility of squarephaneic tetraimide for use as an organic battery electrode material, *Faraday Discuss.* **2024**, *250* (0), 129-144. DOI:10.1039/D3FD00145H
34. Weeraratne, K. S.; Alzharani, A. A.; El-Kaderi, H. M., Redox-Active Porous Organic Polymers as Novel Electrode Materials for Green Rechargeable Sodium-Ion Batteries, *ACS Appl. Mater. Interfaces* **2019**, *11* (26), 23520-23526. DOI:10.1021/acsami.9b05956
35. Liu, X.; Liu, C.-F.; Lai, W.-Y.; Huang, W., Porous Organic Polymers as Promising Electrode Materials for Energy Storage Devices, *Adv. Mater. Technol.* **2020**, *5* (9), 2000154. DOI:10.1002/admt.202000154
36. Zhang, L.; Wang, R.; Liu, Z.; Wan, J.; Zhang, S.; Wang, S.; Hua, K.; Liu, X.; Zhou, X.; Luo, X.; Zhang, X.; Cao, M.; Kang, H.; Zhang, C.; Guo, Z., Porous Organic Polymer with Hierarchical Structure and Limited Volume Expansion for Ultrafast and Highly Durable Sodium Storage, *Adv. Mater.* **2023**, *35* (17), 2210082. DOI:10.1002/adma.202210082
37. Dantas, R.; Ribeiro, C.; Souto, M., Organic electrodes based on redox-active covalent organic frameworks for lithium batteries, *Chem. Commun.* **2024**, *60* (2), 138-149. DOI:10.1039/D3CC04322C
38. Kim, J.; Ling, J.; Lai, Y.; Milner, P. J., Redox-Active Organic Materials: From Energy Storage to Redox Catalysis, *ACS Mater. Au* **2024**. DOI:10.1021/acsmaterialsau.3c00096
39. Peterson, E.; Maust, R. L.; Jasti, R.; Kertesz, M.; Tovar, J. D., Splitting the Ring: Impact of Ortho and Meta Pi Conjugation Pathways through Disjointed [8]Cycloparaphenylene Electronic Materials, *J. Am. Chem. Soc.* **2022**, *144* (10), 4611-4622. DOI:10.1021/jacs.2c00419
40. Bao, Z.; Chan, W. K.; Yu, L., Exploration of the Stille Coupling Reaction for the Synthesis of Functional Polymers, *J. Am. Chem. Soc.* **1995**, *117* (50), 12426-12435. DOI:10.1021/ja00155a007
41. Littke, A. F.; Schwarz, L.; Fu, G. C., Pd/P(t-Bu)3: A Mild and General Catalyst for Stille Reactions of Aryl Chlorides and Aryl Bromides, *J. Am. Chem. Soc.* **2002**, *124* (22), 6343-6348. DOI:10.1021/ja020012f
42. Moro, S.; Spencer, S. E. F.; Lester, D. W.; Nübling, F.; Sommer, M.; Costantini, G., Molecular-Scale Imaging Enables Direct Visualization of Molecular Defects and Chain Structure of Conjugated Polymers, *ACS Nano* **2024**, *18* (18), 11655-11664. DOI:10.1021/acsnano.3c10842
43. Vanderspikken, J.; Liu, Z.; Wu, X.; Beckers, O.; Moro, S.; Quill, T. J.; Liu, Q.; Goossens, A.; Marks, A.; Weaver, K.; Hamid, M.; Goderis, B.; Nies, E.; Lemaur, V.; Beljonne, D.; Salleo, A.; Lutsen, L.; Vandewal, K.; Van Mele, B.; Costantini, G.; Van den Brande, N.; Maes, W., On the Importance of Chemical Precision in Organic Electronics: Fullerene Intercalation in Perfectly Alternating Conjugated Polymers, *Adv. Funct. Mater.* **2023**, *33* (52), 2309403. DOI:10.1002/adfm.202309403
44. Rimmele, M.; Qiao, Z.; Panidi, J.; Furlan, F.; Lee, C.; Tan, W. L.; McNeill, C. R.; Kim, Y.; Gasparini, N.; Heeney, M., A polymer library enables the rapid identification of a highly scalable

and efficient donor material for organic solar cells, *Mater. Horiz.* **2023**, *10* (10), 4202-4212. DOI:10.1039/D3MH00787A

45. Ye, L.; Li, W.; Guo, X.; Zhang, M.; Ade, H., Polymer Side-Chain Variation Induces Microstructural Disparity in Nonfullerene Solar Cells, *Chem. Mater.* **2019**, *31* (17), 6568-6577. DOI:10.1021/acs.chemmater.9b00174
46. Ponder Jr, J. F.; Chen, H.; Luci, A. M. T.; Moro, S.; Turano, M.; Hobson, A. L.; Collier, G. S.; Perdigão, L. M. A.; Moser, M.; Zhang, W.; Costantini, G.; Reynolds, J. R.; McCulloch, I., Low-Defect, High Molecular Weight Indacenodithiophene (IDT) Polymers Via a C–H Activation: Evaluation of a Simpler and Greener Approach to Organic Electronic Materials, *ACS Mater. Lett.* **2021**, *3* (10), 1503-1512. DOI:10.1021/acsmaterialslett.1c00478
47. Warr, D. A.; Perdigão, L. M. A.; Pinfold, H.; Blohm, J.; Stringer, D.; Leventis, A.; Bronstein, H.; Troisi, A.; Costantini, G., Sequencing conjugated polymers by eye, *Sci. Adv. 4* (6), eaas9543. DOI:10.1126/sciadv.aas9543
48. Li, P.; Ding, F., Origin of the herringbone reconstruction of Au(111) surface at the atomic scale, *Sci. Adv. 8* (40), eabq2900. DOI:10.1126/sciadv.abq2900
49. Écija, D.; Otero, R.; Sánchez, L.; Gallego, J. M.; Wang, Y.; Alcamí, M.; Martín, F.; Martín, N.; Miranda, R., Crossover Site-Selectivity in the Adsorption of the Fullerene Derivative PCBM on Au(111), *Angew. Chem., Int. Ed.* **2007**, *46* (41), 7874-7877. DOI:10.1002/anie.200702531
50. Della Pia, A.; Riello, M.; Floris, A.; Stassen, D.; Jones, T. S.; Bonifazi, D.; De Vita, A.; Costantini, G., Anomalous Coarsening Driven by Reversible Charge Transfer at Metal–Organic Interfaces, *ACS Nano* **2014**, *8* (12), 12356-12364. DOI:10.1021/nn505063w
51. Hanwell, M. D.; Curtis, D. E.; Lonie, D. C.; Vandermeersch, T.; Zurek, E.; Hutchison, G. R., Avogadro: an advanced semantic chemical editor, visualization, and analysis platform, *J. Cheminform.* **2012**, *4* (1), 17. DOI:10.1186/1758-2946-4-17
52. Gobalasingham, N. S.; Thompson, B. C., Direct arylation polymerization: A guide to optimal conditions for effective conjugated polymers, *Prog. Polym. Sci.* **2018**, *83*, 135-201. DOI:10.1016/j.progpolymsci.2018.06.002
53. Hendriks, K. H.; Li, W.; Heintges, G. H. L.; van Pruissen, G. W. P.; Wienk, M. M.; Janssen, R. A. J., Homocoupling Defects in Diketopyrrolopyrrole-Based Copolymers and Their Effect on Photovoltaic Performance, *J. Am. Chem. Soc.* **2014**, *136* (31), 11128-11133. DOI:10.1021/ja505574a
54. Schleyer, P. v. R.; Maerker, C.; Dransfeld, A.; Jiao, H.; van Eikema Hommes, N. J. R., Nucleus-Independent Chemical Shifts: A Simple and Efficient Aromaticity Probe, *J. Am. Chem. Soc.* **1996**, *118* (26), 6317-6318. DOI:10.1021/ja960582d
55. Plasser, F.; Glöcklhofer, F., Visualisation of chemical shielding tensors (VIST) to elucidate aromaticity and antiaromaticity, *Eur. J. Org. Chem.* **2021**, *2021*, 2529-2539. DOI:10.1002/ejoc.202100352

56. Plasser, F.; Wormit, M.; Dreuw, A., New tools for the systematic analysis and visualization of electronic excitations. I. Formalism, *J. Chem. Phys.* **2014**, *141* (2), 024106. DOI:10.1063/1.4885819
57. Plasser, F., Exploitation of Baird Aromaticity and Clar's Rule for Tuning the Triplet Energies of Polycyclic Aromatic Hydrocarbons, *Chemistry* **2021**, *3* (2), 532-549. DOI:10.3390/chemistry3020038

TOC Graphic: